American Journal of Mechanical Engineering, 2024, Vol. 12, No. 3, 35-43
Available online at http://pubs.sciepub.com/ajme/12/3/2
Published by Science and Education Publishing
DOI:10.12691/ajme-12-3-2

Optimization of Seatbelt Restraint Forces in Vehicle Frontal Crashes

Fenghui SHI*

Department of Mechanical Engineering, National Institute of Technology, Akashi College,
Japan 679-3 Nishioka, Uozumi-cho, Akashi, Hyogo 674-8501, Japan
*Corresponding author: shi@akashi.ac.jp

Received August 19, 2024; Revised September 21, 2024; Accepted September 28, 2024

Abstract Current seat belt systems use a force limiter mechanism. However, they have the disadvantage of being unable to accommodate a wide range of speeds, as they provide constant performance regardless of speed. The purpose of this study is to reduce restraint forces across a wide range of speeds by developing a semi-active vehicle seatbelt system using a Magneto-Rheological (MR) shock absorber. The effect of system response delay is also considered. In this study, a vehicle model for the sled test is proposed for simulation and MR shock absorber optimization. In the first step, we optimized the gap of the MR valve and the initial pressure of the gas chamber. Then, the current applied to the coil is fine-tuned by minimizing restraint forces for various frontal crash speeds. The results show that the seat belt system with an MR shock absorber can significantly reduce restraint forces for various crash speeds. In all cases-Case 1, Case 2, and Case 3-by optimizing the current value *I*, the maximum chest restraint force was reduced by approximately 13.6% to 52.5% compared to using only the seatbelt.

Keywords: *seatbelt, optimization, MR Fluid, Seatbelt Restraint Forces, MR Damper, Semi-active seatbelt*

Cite This Article: Fenghui SHI, "Optimization of Seatbelt Restraint Forces in Vehicle Frontal Crashes." *American Journal of Mechanical Engineering*, vol. 12, no. 3 (2024): 35-43. doi: 10.12691/ajme-12-3-2.

1. Introduction

Seat belts can save lives. Restraints in vehicles have prevented innumerable deaths due to a head injury and many other lethal fates [1].

The first seat belt designs were introduced in 1894, after being patented in 1885. In motor vehicles, the front lap belt became standard in 1964. In 1973 the lap belt was upgraded to a three-point harness, mostly due to the efforts of Bohlin. This introduction has led to almost a 50% decrease in fatal injuries from automobile collisions [2]. Safety harnesses represent "active restraints," while airbags and head restraints are referred to as passive restraints. Despite obvious benefits, seat belts are not universally used in most countries. The National Highway Traffic Safety Administration (NHTSA) reported an 83% compliance in the United States in 2008 [3].

Although seatbelts have prevented numerous deaths by reducing head injuries, they can cause damage via the transmission of force upon impact associated with the restraint of a passenger. Seatbelt injury, also called seatbelt syndrome. The three-point adult harness rests on the shoulder, chest, and abdomen.

Current seat belts are equipped with pretensioner and force limiter mechanisms. The pretensioner mechanism quickly retracts the belt in the event of a frontal collision, accelerating the occupant's restraint. The force limiter mechanism gradually loosens the seat belt under a certain load to prevent excessive force on the occupant's chest, thereby providing protection. However, this force limiter mechanism is generally a passive system that provides consistent performance regardless of speed. As shown in Figure 1, the fatal and serious injury rates for chest injuries remain nearly constant once the simulated speed exceeds 60 km/h. This is likely due to the force limiter being in effect. Furthermore, the significant increase in the fatal and serious injury rates for head injuries when the simulated speed exceeds 80 km/h suggests that insufficient restraint by the force limiter leads to increased occupant displacement and secondary collisions with the steering wheel or other parts. Thus, it can be said that conventional force limiter mechanisms have the drawback of not being able to accommodate a wide range of speeds.

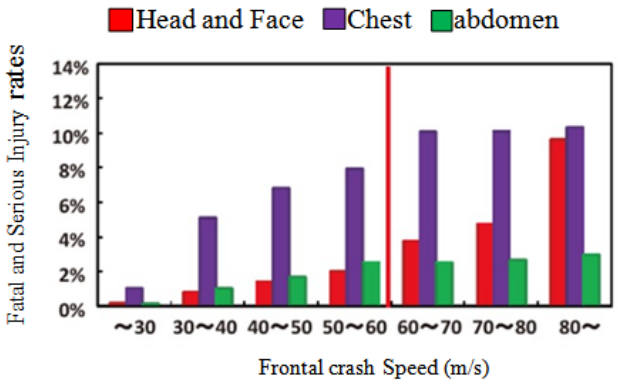

Figure 1. Fatal and Serious Injury rates vs Frontal crash Speed (m/s) [4]

Adaptive seat belts are able to adjust their configuration during, or before, the secondary collision. In this way, the protection could be made optimal for a specific occupant, occupant position, vehicle, or crash (Mackay et al.,1994) [5]. This flexibility allows improving the occupant's response for the actual situation. The need to develop intelligent, real-time controlled restraint systems has also been recognized in the roadmap for future passive safety technology (Wismans, 2007) [5].

The term adaptive seat belts is adhered to, but different names can be found in literature (Wismans, 2003) [7]. They are also called smart, intelligent or active seat belts, although these terms do not systematically refer to different systems. Differences can, however, be seen in the approaches that are used, and three types of adaptive systems can be distinguished.

This study explores the possibility of reducing chest restraint forces by incorporating a semi-active mechanism using MR dampers into the seat belt system. We proposed an optimization method to minimize restraint forces with the MR damper. In the first step, MR damper parameters are optimized, and in the second step, the optimal current values are determined for different crash speeds.

1. At a low collision speed (30 km/h), the structure of the MR damper is optimized without applying current to the MR damper's coil.
2. For collision speeds ranging from 40 to 80 km/h, the optimal current values are determined through optimization, allowing the system to accommodate a wide range of collision speeds.
3. The system response delay and other factors are considered to investigate how much they affect the restraint force and to determine acceptable limits.

2. Dynamic Model of Seatbelt System

Dynamic model proposed used to study the dynamic of the human thorax in a crash of a vehicle is shown in Figure 2 where the vehicle is shaded. In this model, m_1 is the effective mass of the sternum and a portion of the anterior rib cage and thoracic contents, m_2 is the effective mass of seatbelt systems. x_1, x_2 are displacements respectively. X is displacement of vehicle body. Accelerations change of vehicle body is half-cycle sine wave (Figure 3). MR damper in Figure 2 is a damper filled with magnetorheological fluid, which is controlled by a magnetic field, usually using an electromagnet [8,9,10]. This allows the damping characteristics of the damper to be continuously controlled by varying the power of the electromagnet. The damping force can be controlled by MR fluid viscosity increases within the damper as electromagnet intensity increases.

The vehicle model is shown in Figure 2. This model is designed for a sled test, simulating and optimizing by applying a half-cycle sine wave acceleration to the vehicle from the front. In this simulation, six different crash speeds are set: 30, 40, 50, 60, 70, and 80 km/h, as these speeds were determined to be the most practical.

The following assumptions are made for the simulation: (1) The crash type is a frontal (full-lap) collision; (2) The human mass considered is limited to the thorax, and only translational motion is taken into account; (3) The vehicle collision is assumed to end 0.08 seconds after the initial impact.

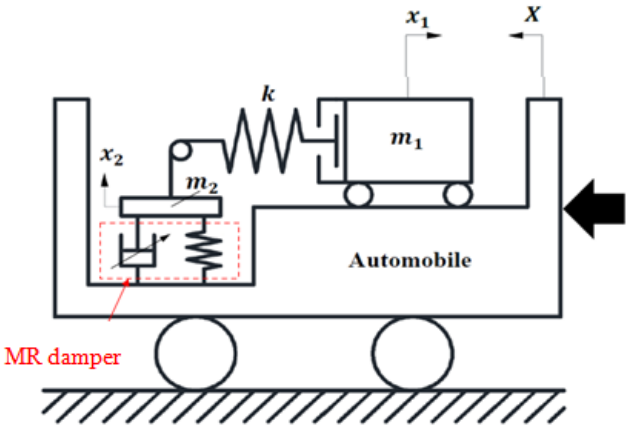

Figure 2. Dynamic Model

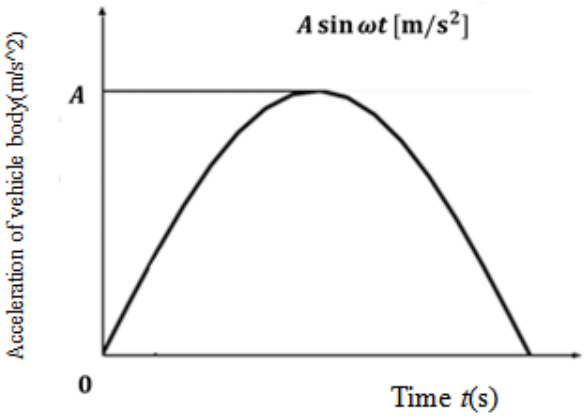

Figure 3. Acceleration of vehicle body

Based on Figure 2, the equations of motion are as follows.

$$m_1\ddot{x}_1 = -F \tag{1}$$

$$m_2\ddot{x}_2 = F - F_d - F_k \tag{2}$$

Where F is restraint force to the human thorax, F_d and F_k are the damping force of the MR damper and the restoring force from the air spring. F_d and F_k will be described in the next section.

$$F = k(x_1 - x_2 + X) \tag{3}$$

X and k represent the vehicle displacement and the restoring spring constant of the seat belt, respectively.

The vehicle body acceleration due to a half-cycle sine wave is expressed as follows:

$$\ddot{X} = A\sin\omega t \qquad (0 \le t \le \pi/\omega) \tag{4}$$

$$A = \frac{\pi v_0}{2t_p} \tag{5}$$

$$\omega = \frac{\pi}{t_p} \tag{6}$$

A and ω are the amplitude and angular velocity of the half-cycle sine wave used for the body acceleration. v_0 is the collision speed, and t_p is the collision end time.

3. MR Damper

In this section, the quasi-static model of MR valves is presented. The equations are derived based on the assumption that the MR fluid exhibits Bingham plastic behavior and the flow is fully developed in the ducts [11,12]. As shown in Figure 4, the MR valve structure includes the outer and inner pistons which divide the MR damper into upper and lower champers. Both champers are fully filled with MR fluids. As the inner piston moves, the MR fluid flows from one champers to the other one through the orifice of the valve. Significant geometrical parameters of the MR valve are the valve height L, the valve mean diameter of the annular MR fluid gap d_m, the valve orifice gap h and the pole length t_b, which are presented in Figure 5.

When the coil is electrified, a magnetic circuit appears as shown in the figure. At the two end flanges, flux lines are perpendicular to the flow direction which causes a field−dependent resistance on the flow. The pressure drop developed in such kind of MR valve is given by [11,12,15].

$$\Delta P = \Delta P_\eta + \Delta P_\tau = \frac{6\eta L}{\pi h^3 d_m} Q + 2c \frac{t_b}{h} \tau_y \qquad (7)$$

Here, Q is the volumetric flow rate, η is the viscosity without a magnetic field, τ_y is the yield stress induced by the magnetic field The parameter c is a coefficient dependent on the velocity distribution, and it varies between 2.07 and 3.07. The parameter c can be approximated as follows [12]:

$$c = 2.07 + \frac{12Q\eta}{12Q\eta + 0.4\pi h^2 \tau_y} \qquad (8)$$

The second term of Equation (7) can be continuously controlled by the strength of the magnetic field passing through the MR valve's gap. This is a dominant term in damping force and is expected to have a significant impact on the design of the MR damper. The yield stress τ_y generated in the MR fluid due to the applied magnetic field is typically characterized for various MR fluids. In this study, the MR fluid "MRF-140BC," (Lord Corporation), will be used. Figure 6 shows the data sheet for this MR fluid. The experimentally obtained yield stress τ_y [Pa] for this MR fluid can be approximated as a function of the applied magnetic field strength H_{mr} (A/m) as follows:

$$\tau_y = C_0 + C_1 H_{mr} + C_2 H_{mr}^2 \qquad (9)$$

The coefficients C_0, C_1 and C_2 are -481.69, 0.31543, and - 3.216×10^{-7}, respectively.

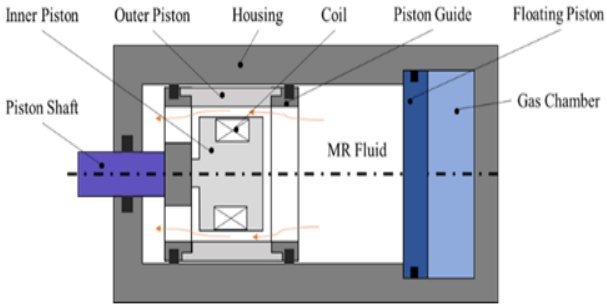

Figure 4. Schematic configuration of MR damper [13]

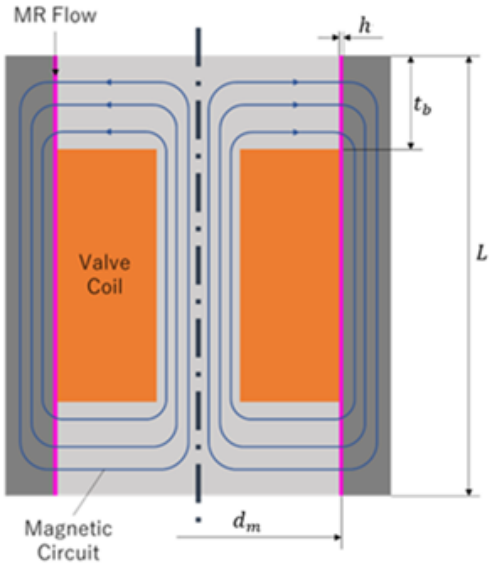

Figure 5. Coil of MR valve [14]

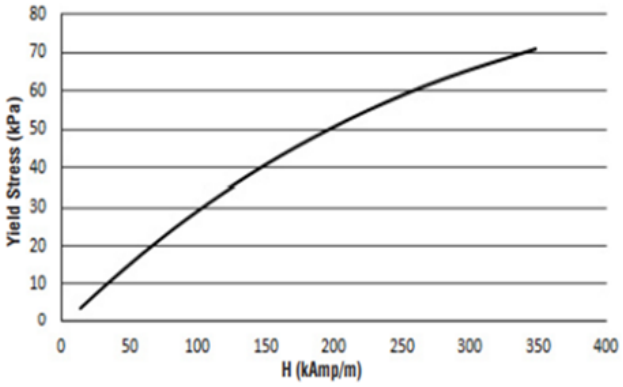

Figure 6. Yield Stress vs. Magnetic Field Intensity [16]

Based on Kirchhoff's laws and the magnetic flux conservation principle for the magnetic circuit, and assuming that the magnetic field strength along the effective length of each link in the magnetic circuit is constant, the relationship between the magnetic field strength H_{mr} in the MR fluid and the applied current I can be approximated as follows.

$$H_{mr} = \frac{N_c I}{2h} \qquad (10)$$

N_c, h, and I represent the number of turns of the coil, the gap of the MR valve, and the current flowing through the coil, respectively.

The damping force of the MR damper is determined by the damper's shape, input current, characteristics of the MR fluid, and the movement of the damper. Assuming the behavior of the MR damper is quasi-static and neglecting frictional forces, the damping force of the MR damper can be obtained using the following equation

$$F_d = P_2 A_p - P_1(A_p - A_s) \tag{11}$$

A_p and A_s represent the effective cross-sectional areas of the piston and piston shaft, respectively. $P_1$and P_2 are the pressures in the upper and lower chambers of the MR damper, respectively. If the pressure in the gas chamber P_a is approximated to be equal to the pressure in the lower chamber P_2, it can be expressed as follows:

$$P_1 = P_a - \Delta P \tag{12}$$

$$P_2 = P_a \tag{13}$$

The pressure in the gas chamber can be determined using the following equation:

$$P_a = P_0 \left(\frac{V_0}{V_0 - A_s x_2} \right)^{\gamma} \tag{14}$$

Here, P_0 and V_0 represent the initial pressure and volume of the gas chamber, respectively. The parameter γ represents the thermal expansion coefficient and varies between 1.4 and 1.7. Based on Equations (11) to (13), the damping force of the MR damper can be described as follows:

$$F_d = P_a A_p - \Delta P(A_p - A_s) \tag{15}$$

Additionally, the restoring force of the air spring is given by the following equation:

$$F_k = P_a A_p \tag{16}$$

4. Optimization

In this section, the optimization method is introduced. There two steps for this optimization. The algorithm used is the "genetic algorithm." Initial Values for MR Damper Design are expressed in Table 1.

MATLAB/Simulink2020b is used in optimization and Simulation [18,19,20].

See Appendices about block diagrams (Figure 12 Figure 13 Figure 14 Figure 15).

4.1. Optimization of the Parameters of the MR Damper

In the first step, the parameters of the MR damper, including the gap h of the MR valve and the initial pressure P_0 of the gas chamber (Figure 4 and Figure 5), will be optimized without applying the magnetic circuit.

The objective function for this optimization is given by Equation (17), which aims to minimize the maximum restraint force applied to the chest. The design variables and the constraints are defined by Equations (18) and (19).

Table 1. Initial Values for MR Damper Design

Symbols	Units	Values	Symbols	Units	Values
m_1	kg	17.19	L	m	0.05
m_2	kg	5.0	A_p	m^2	2.826×10^{-3}
t_p	s	0.08	A_s	m^2	7.854×10^{-5}
g	m/s^2	9.8	η	$P_a\cdot$ s	0.114
k	N/m	80000	N_c	Turns	10^3
w	rad/s	39.3	P_0	P_a	10^5
t_b	m	0.015	v_0	m^3	2.826×10^{-4}
d_m	m	0.049	γ		1.4

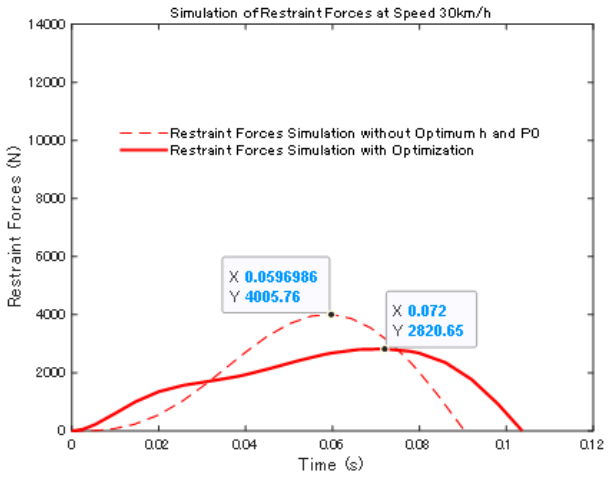

Figure 7. Comparison of Restraint Forces

The objective function

$$f(x) = \min(\max F) \tag{17}$$

The design variables

$$x = (x_1, x_2)^T = (h, P_0)^T \tag{18}$$

The constraints

$$\begin{cases} 0.0001 \le x_1 \le 0.003 \\ 50000 \le x_2 \le 500000 \end{cases} \tag{19}$$

The optimization results are

$h^* = 0.0018$ m, $P_0^* = 498730$ Pa

The simulation results for the optimization of the MR valve gap h and the initial pressure P_0 of the gas chamber at impact speed 30 km/h are shown in Figure 7. As demonstrated by these results, using the optimum MR damper reduced the restraint force about 29.6%.

Using the result optimum h^* and P_0^*, the 2nd step optimization for impact speed at 40, 50, 60, 70, 80km/h will be done in the next section.

4.2. Optimization of Current

In the 2nd step, the current value I corresponding to each collision speed applied to the coil, will be optimized.

The optimization method employed in this study is described below.

The applied current I to the coil is expressed as a piecewise linear function in Figure 8 (Case1, Case2, Case3). The crash termination time of 0.08 seconds is divided into intervals of 0.02 seconds. The reason for dividing into 0.02-second intervals is to account for the response time of the MR fluid, which takes a few milliseconds, and to capture the characteristics of the current at each crash time interval. A representative current value is set for each of these 0.02-second intervals, and the current value at the i-th representative point is denoted as I_i. The current value after the crash termination time is assumed to remain the same as the representative point value at 0.08 seconds. Thus, it can be expressed by the following equation.

We propose three methods for applying current to the MR fluid. See Figure 8 (Case1, Case2 and Case3)

The objective function is as same as Equation (17).

Case1: The current value remains constant during the crash termination time of 0.08 seconds.

The design variable is expressed as

$$x = I \tag{20}$$

Case2: The current value remains constant during the intervals time, 0.02 seconds.

The design variables are expressed as

$$x_i = I_i (i = 1, 2, 3, 4) \tag{21}$$

Case3: The applied current I to the coil is expressed as a piecewise linear function during the intervals time, 0.02 seconds.

The design variables are expressed as

$$x_i = I_i + \frac{I_{i+1} - I_i}{0.02}\left[t - 0.02(i-1)\right] \tag{22}$$

$$(i = 1, 2, \cdots, 5)$$

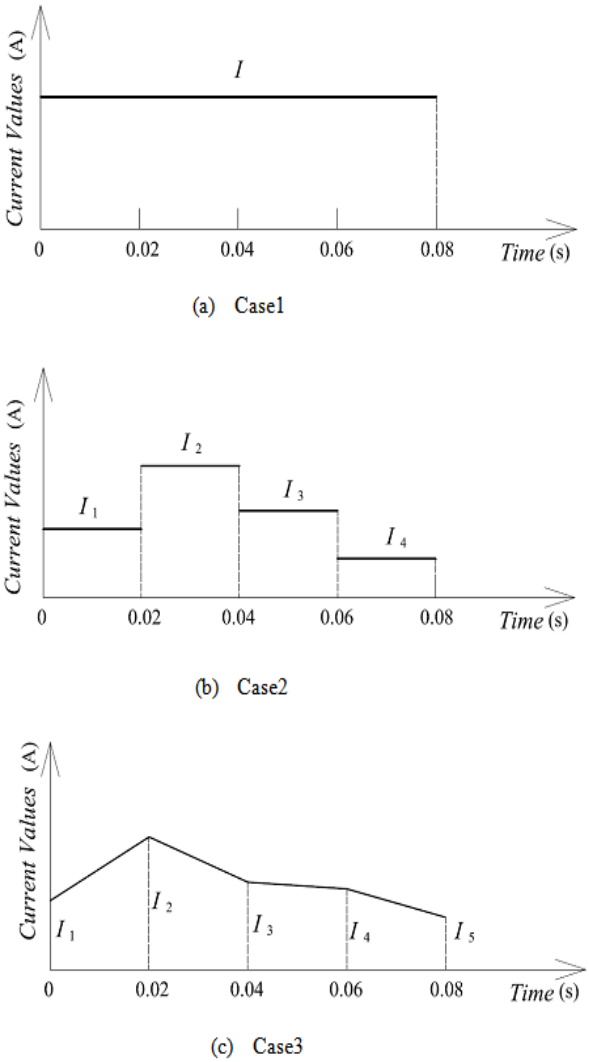

Figure 8. Method for Defining the Applied Current as Design Variables

5. Optimization Results and Discussion

Optimization was performed using a genetic algorithm in cases 1, 2, and 3. The optimization results are shown in Table 1, Table 2, and Table 3. The simulation results for seat belt restraint forces at different collision speeds are shown in Figure 9, Figure 10, and Figure 11. For collision speeds below 30 km/h, no current is applied to the MR damper. For collision speeds between 40 km/h to 80 km/h, optimal current is applied to the MR damper. By applying this optimal current to the MR damper, the seat belt's restraint force can be controlled, and by distributing the maximum restraint force over the collision period (0.08s), the peak value of the restraint force can be reduced. The vehicle can remain in standby mode, adjusting the corresponding current according to the driving speed.

Table 1 shows the optimization results for Case 1. During the collision period (Figure 8(a)), the current value remains constant. The maximum restraint force when current is applied is smaller than when no current is applied. However, the reduction rate is the smallest among the three cases, with a maximum reduction of 39.2% and a minimum reduction of 13.6%.

Table 2 shows the optimization results for Case 2. During the collision period (0.08s), the current value remains constant every 0.02s (Figure 8(b)). The maximum restraint force when current is applied is reduced by a maximum of 49.5% and a minimum of 28.1% compared to when no current is applied.

Table 3 shows the optimization results for Case 3. During the collision period (0.08s), the current value changes every 0.02s (Figure 8(c)). The maximum restraint force when current is applied is reduced by a maximum of 52.5% and a minimum of 43.5% compared to when no current is applied. This case achieves the greatest reduction in maximum restraint force among the three cases.

Table 2. Optimization Results of Case1

.	Optimum Currents Values I_i^*(A)	Maximum Restraint Forces (N)		the reduction ratio
		With Optimum MR Damper	Without Optimum MR Damper	
8.333 (30km/h)	0	2820.65	4005.76	-29.6%
11.11 (40km/h)	0.1124	3982.38	4606.96	-13.6%
13.89 (50km/h)	0.1871	4982.04	6933.56	-28.1%
16.67 (60km/h)	0.2701	6000.02	9198.71	-34.8%
19.44 (70km/h)	0.3617	7021.49	11232.7	-37.5%
22.22 (80km/h)	0.4625	8048.37	13235.7	-39.2%

Table 3. Optimization Results of Case2

Collision Speed (m/s)	Optimum Currents Values I_i^*(A)	Maximum Restraint Forces (N)		the reduction ratio
		With Optimum MR Damper	Without Optimum MR Damper	
8.333 (30km/h)	0, 0, 0 ,0	2820.65	4005.76	-29.6%
11.11 (40km/h)	2.213, 0.4749, 0.3102, 0.0634	3313.7	4606.96	-28.1%
13.89 (50km/h)	1.365, 0.4771, 0.2354, 0.5510	4188.06	6933.56	-39.6%
16.67 (60km/h)	2.012, 2.999, 0.1908, 0.3302	5101.53	9198.71	-44.5%
19.44 (70km/h)	2.211, 2.999, 0.2281, 0.4156	5842.04	11232.7	-48.0%
22.22 (80km/h)	1.836, 0.4732, 0.3339, 0.2923	6679.53	13235.7	-49.5%

Table 4. Optimization Results of Case3

Collision Speed (m/s)	Optimum Currents Values I_i^*(A)	Maximum Restraint Forces (N)		The reduction ratio
		With Optimum MR Damper	Without Optimum MR Damper	
8.333 (30km/h)	0, 0, 0 ,0, 0	2820.65	4005.76	-29.6%
11.11 (40km/h)	1.773, 0.2574, 0.1114, 0.0272, 0.1239	2604.58	4606.96	-43.5%
13.89 (50km/h)	2.525, 0.3203, 0.1216, 0.334, 0.0103	3294.59	6933.56	-52.5%
16.67 (60km/h)	2.511, 0.4865, 0.2216, 0.1307, 0.2552	4493.66	9198.71	-51.1%
19.44 (70km/h)	2.401, 1.278, 0.1194, 0.3947, 0.0607	5909.81	11232.7	-47.4%
22.22 (80km/h)	2.331, 0.9283, 0.4299, 0.2004, 0.9602	6841.52	13235.7	-48.3%

Regarding the optimal current values, Case 1 requires the smallest current (0.1124A to 0.4635A), while Case 2 and Case 3 require higher current values, ranging from 1.365A to 2.525A.

Figure 9, Figure 10, and Figure 11 show the simulation results. For Case 1 (Figure 9), all the restraint force curves for collision speeds ranging from 30 km/h to 80 km/h are flat and smooth.

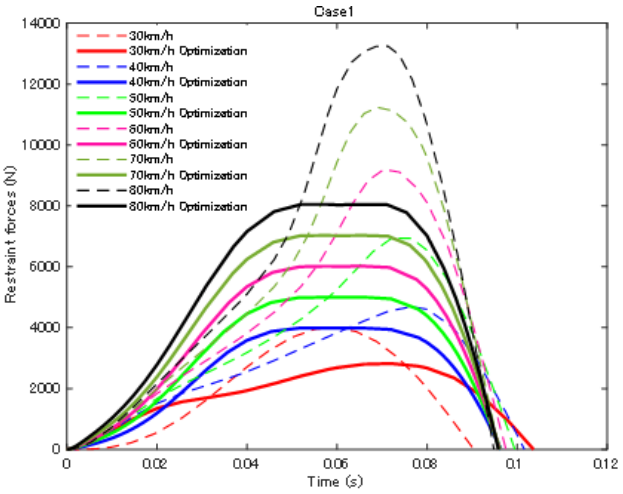

Figure 9. Comparison of Restraint Forces for case1

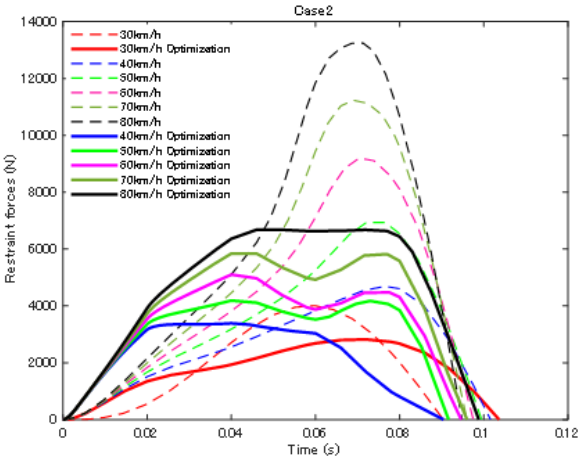

Figure 10. Comparison of Restraint Forces for case2

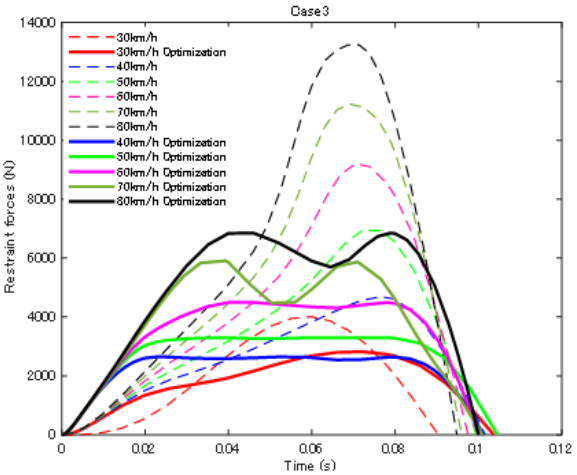

Figure 11. Comparison of Restraint Forces for case3

Figure 10 and Figure 11 express the simulation results for Case 2 and Case 3. Although the maximum restraint forces are smaller than those in Case 1, the 60 km/h (pink solid line) and 70 km/h (green solid line) curves in Figure 10, and the 70 km/h (green solid line) and 80 km/h (black solid line) curves in Figure 11 exhibit some fluctuations.

Regarding current control, Case 1 is considered simple, while Case 3 is more complex.

6. Conclusions

A seatbelt system model with an MR damper was constructed, and three control methods were proposed in this study. Effective optimization was performed for Case 1, Case 2, and Case 3, and the current applied to the MR fluid for different collision speeds was calculated.

By optimizing the MR valve gap h and the initial pressure P_0 of the gas chamber, a reduction in restraint force was observed. It was clear from equations (7) and (8) that the gap significantly affects the damping force of the MR damper. However, at the initial stage of the collision, the initial pressure P_0 of the gas chamber is also considered to have a substantial impact.

In all cases-Case 1, Case 2, and Case 3-by optimizing the current value I, the maximum chest restraint force was reduced by approximately 13.6% to 52.5% compared to using only the seatbelt. Furthermore, the shape of the graph also became more ideal.

References

[1] Campbell BJ. Safety belt injury reduction related to crash severity and front seated position. J Trauma. 1987 Jul; 27(7): 733-9.

[2] Porter RS, Zhao N. Patterns of injury in belted and unbelted individuals presenting to a trauma center after motor vehicle crash: seat belt syndrome revisited. Ann Emerg Med. 1998 Oct; 32(4): 418-24.

[3] Thoma T. National Highway Traffic Safety Administration (NHTSA) Notes. Review of studies on pedestrian and bicyclist safety, 1991-2007. Ann Emerg Med. 2012 Oct; 60(4): 495-6.

[4] Research on Improving the Accuracy of Collision Speed Estimation for Front and Rear Impact Accidents, Report of Institute for Traffic Accident Research and Data Analysis, Japan. 2012.

[5] Mackay, M. (1994). Smart seat belts - Some population considerations applied to intelligent restraint systems. In Proceedings of the SAE International Congress and Exposition, 28 Feb - 3 Mar, Detroit, MI, USA, paper nr. 940531 in SAE Technical Papers, p. 13–22.

[6] Wismans, J. S. H. M. (2007). Secondary Safety Research Action Plan - Updated Roadmap. Technical Report D40, Advanced Passive Safety Network (ASPN).

[7] Wismans, J. S. H. M. (2003). State-of-the-art report: Smart Restraint Systems. Task 5 report, European Vehicle Passive Safety Network.

[8] "Innovative Designs for Magneto-Rheological Dampers" (PDF). Retrieved 2013-12-08.

[9] Primary Suspension Archived October 14, 2007, at the Wayback Machine http:// www.lord.com/ Home Magneto RheologicalMR Fluid/MRFluidTechnology/tabid/3318/Default.aspx MR Fluid Technology Archived October 13, 2007, at the Wayback Machine.

[10] Nguyen, Q. H. Han, Y. M. Choi, S.B. and Wereley, N.M. "Geometry optimization of MR valves constrained in a specific volume using the finite element method," Smart Materials and Structures, 2007. 16: p. 2242–2252.

[11] Jolly, M. R. Bender, J.W. and Carlson, J.D. "Properties and applications of commercial magnetorheological fluids," 1998, Thomas Lord Research Center, Lord Corporation. p. 262-275.

[12] Nguyen, Q. H. and Choi, S. B. "Optimal design of MR shock absorber and application to vehicle suspension," Smart Materials and Structures, 2009. 18: p. 035012-22.

[13] Nguyen, Q. H., Han, Y. M., Choi, S.B. and Wereley, N.M. "Geometry optimization of MR valves constrained in a specific volume using the finite element method," Smart Materials and Structures, 2007. 16: p. 2242–2252.

[14] Nguyen, Q. H. Choi, S.B. and Wereley, N.M. "Optimal design of magnetorheological valves via a finite element method considering control energy and a time constant," Smart Materials and Structures, 2008. 17: p. 025024-36.

[15] LORD TECHNICAL DATA Sheet, MRF-140CG Magneto-Rheological Fluit. https:// assets.website-files.com / 612e162206d570eec03114fb/61716f81b70b5236eabcded4_DS7012_MRF-140CG.pdf.

[16] Yang X, Shi J, Fu Q, Pu S, Lian C, Li K, Yin Z, Liu S and Wang G (2022), Optimization of the driver's seat belt and injury biomechanical analysis in real world minivan small offset impact accident scenarios, Front. Bioeng. Biotechnol, 10: 965206.

[17] Song, C.Y. Enhanced Robust Design Optimization in Seat Belt Anchorage Strength for Front Crash Safety of Multi-Purpose Vehicle. Appl. Sci. 2021, 11, 1023.

[18] Fenghui Shi, "Formulation and Simulation for Speed Control Humps." American Journal of Mechanical Engineering, vol. 12, no. 3 (2024): 26-34.

[19] Fenghui Shi, "Multi-objective Optimization of Passive Shock Absorber for Landing Gear." American Journal of Mechanical Engineering, vol. 7, no. 2 (2019): 79-86.

[20] Fenghui Shi, Warren Isaac Anak Dean, and Taikei Suyama, "Single-objective Optimization of Passive Shock Absorber for Landing Gear." American Journal of Mechanical Engineering, vol. 7, no. 3 (2019): 107-115.

Appendices

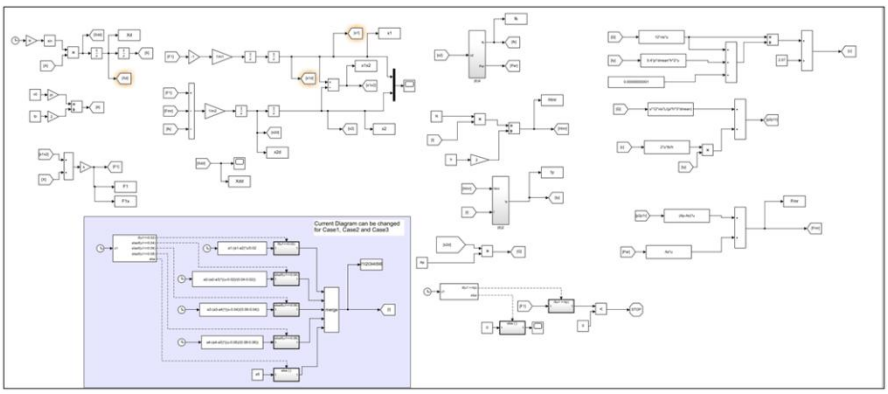

Figure 12. MATLAB/Simulink Block Diagram of the Seatbelt Model

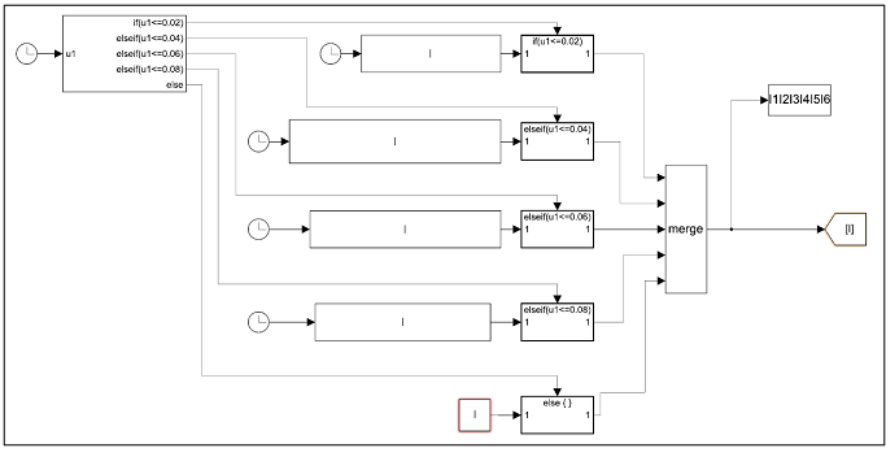

Figure 13. Currents Block Diagram of Case1

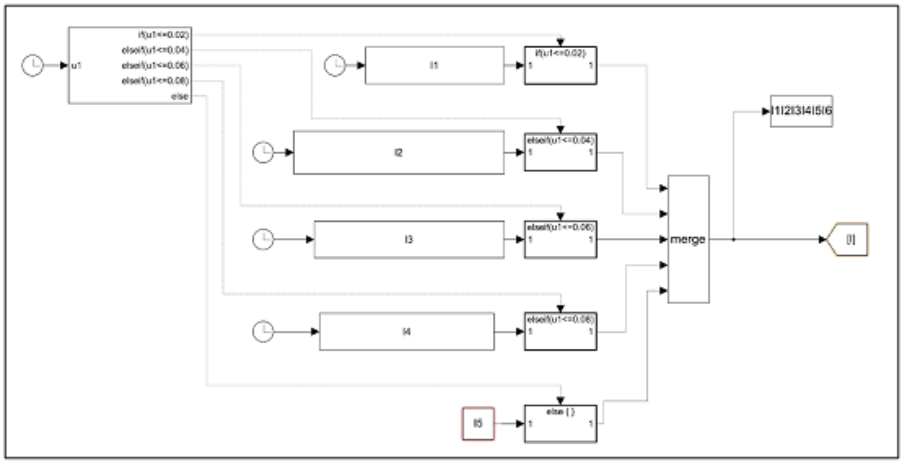

Figure 14. Currents Block Diagram of Case2

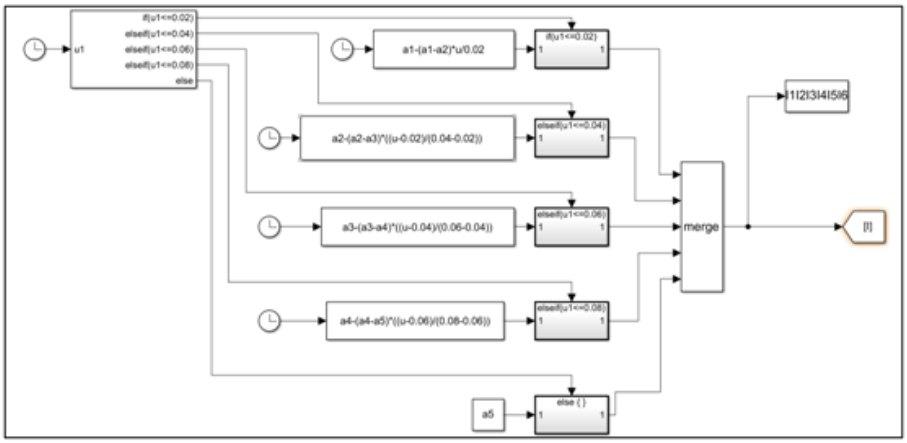

Figure 15. Currents Block Diagram of Case3